

# Doubly stochastic models for replicated spatio-temporal point processes

Daniel Gervini

Department of Mathematical Sciences  
University of Wisconsin–Milwaukee

March 25, 2019

## Abstract

This paper proposes a log-linear model for the latent intensity functions of a replicated spatio-temporal point process. By simultaneously fitting correlated spatial and temporal Karhunen–Loève expansions, the model produces spatial and temporal components that are usually easy to interpret and capture the most important modes of variation and spatio-temporal correlation of the process. The asymptotic distribution of the estimators is derived. The finite sample properties are studied by simulations. As an example of application, we analyze bike usage patterns on the Divvy bike sharing system of the city of Chicago.

*Key words:* Bike-sharing system; Karhunen–Loève decomposition; latent-variable model; Poisson process.

# 1 Introduction

Point processes in time and space have a broad range of applications, in areas as diverse as neuroscience, ecology, finance, seismology, and many others. Examples are given in classic texts like Baddeley (2007), Cox and Isham (1980), Diggle (2013), Møller and Waagepetersen (2004) and Streit (2010). Due to the prevailing types of data and applications, the point-process literature has mainly focused on single realizations of point processes, such as the distribution of cells in a single tissue sample (Diggle et al., 2006). Spatio-temporal processes, in particular, have been widely studied in the literature (see e.g. Li and Guan, 2014; Shirota and Gelfand, 2017; Waagepetersen et al., 2016), but always in the context of single realizations. An exception has been spike train data, where neural activity from several patients, or from the same patient under different trials, is observed (Brown et al., 2004); in such cases we have a replicated point process, that is, a process observed on different subjects or units.

Among the few papers that have addressed replicated point processes in past years we can cite Diggle et al. (1991), Baddeley et al. (1993), Diggle et al. (2000), Bell and Grunwald (2004), Landau et al. (2004), Wager et al. (2004), and Pawlas (2011). Due to their limited amount data, these papers only proposed estimators for summary statistics of the processes (the so-called  $F$ ,  $G$  and  $K$  statistics) rather than the intensity functions that characterize the processes, which would have been much more informative.

The increased availability of complex data has made replicated point processes more common in recent years. For example, bike sharing systems are becoming ubiquitous in large cities around the world (Shaheen et al., 2010). These systems provide short-term bicycle rental services at unattended stations distributed within the city. The Divvy system of the city of Chicago keeps records of every bike trip in the system and makes them publicly available at the Chicago Data Portal website (<https://data.cityofchicago.org>). In this paper (Section 6) we will analyze trips that took place between April 1 and November 30 of 2016, since bike usage considerably decreases during the winter. There were a total of 3,068,211 bike trips and 458 active bike stations in that period. Each bike trip can be seen as an observation  $(t, \mathbf{s})$  of a spatio-temporal process, where  $t$  is the starting time of the trip and  $\mathbf{s}$  its destination. We can see the 244 days between April 1 and November 30 as the  $n$  replications of

the spatio-temporal process. We will focus on trips originating from a single bike station, the one at the intersection of Wrightwood and Ashland avenues, identified as station 166 in the system. We chose this station because it has the median total annual trip count (4,304) among the 458 stations in the system. It is of interest, in this case, to investigate the existence of patterns in the daily distributions of trip start times and destinations. For example, is bike demand distributed uniformly during the day, or does it spike at certain times of the day? And if so, is this pattern similar every day of the week or is there a difference, for instance, between weekdays and weekends? Are trip destinations uniformly distributed in the vicinity of the bike station or do some specific locations attract most trips? And if so, are these temporal and spatial patterns related? For example, do days with an increased bike demand on a given time frame (e.g. early morning) also show trip destinations concentrated in a specific area (e.g. downtown)? Answering these questions is important for an efficient administration of the system, since understanding the patterns of usage of each station helps correct the imbalances in bike distribution that inevitably arise in these systems (Nair and Miller-Hooks, 2011).

Estimating daily spatio-temporal distributions is possible for the methods proposed in this paper because of the availability of replications, which allow ‘borrowing strength’ across several days. Otherwise, estimation of daily intensity functions would not be feasible for these data, where some days only a dozen or so trips take place; such low counts do not allow accurate estimation of temporal intensity functions, let alone spatial ones, if each day is estimated separately from the others.

The idea of ‘borrowing strength’ across replications underlies most Functional Data methods (Ramsay and Silverman, 2005). However, Functional Data Analysis has mostly focused on continuous processes; little work has been done on discrete point processes so far. There is a link, however, between discrete and continuous time processes via the underlying intensity functions, which, although not directly observable, can be seen as realizations of a latent continuous stochastic process. This relationship has been exploited by some authors, but the literature in the area is still scant. We can mention Bouzas et al. (2006, 2007) and Fernández-Alcalá et al. (2012), which have rather limited scopes since they only estimate the mean of a temporal process, not its variability, and Wu et al. (2013), who estimate the mean and the principal components of a temporal process, but their kernel-based methods are not easy to extend to spatial domains.

The author and his collaborators have recently proposed models for replicated temporal or spatial processes (Gervini, 2016; Gervini and Khanal, 2019), and for marked point processes with continuous marks (Gervini and Baur, 2017), but not for jointly spatio-temporal processes. This paper proposes a log-linear model for the latent intensity process. The model is based on the Karhunen–Loève expansion, or principal component decomposition, of stochastic processes. By fitting correlated temporal and spatial Karhunen–Loève expansions simultaneously, the model produces temporal and spatial components that are easy to interpret and capture the most important modes of variation and spatio-temporal correlation of the process. Note that this is not simply a matter of fitting separate temporal and spatial models as in e.g. Gervini (2016) and Gervini and Khanal (2019) and then computing the cross-correlations. If this is done, there will typically appear a ‘size component’ in both models, with a trivially high cross-correlation because overall count is being explained twice. On the other hand, components that are important for explaining variability in the temporal or spatial domains taken separately, may not be optimal for explaining spatio-temporal cross-correlations; the situation, in this sense, is similar to that of principal component analysis versus canonical variates in multivariate analysis (Seber, 2004). Therefore, although there are similarities with Gervini and Khanal (2019), the joint spatio-temporal models we propose here are not straightforward extensions of those.

This paper is organized as follows. The new model is presented in Section 2 and its estimation procedure in Section 3. Asymptotic results for statistical inference are derived in Section 4, and the finite-sample behavior of the method is studied by simulation in Section 5. As an example of application, the Divvy bike data is analyzed in more detail in Section 6.

## 2 Doubly stochastic spatio-temporal model

A spatio-temporal point process  $X$  is a random countable set in  $\mathcal{S} = \mathbb{R} \times \mathbb{R}^2$  (Møller and Waagepetersen, 2004, ch. 2; Streit, 2010, ch. 2). A point process is locally finite if  $\#(X \cap B) < \infty$  with probability one for any bounded  $B \subseteq \mathcal{S}$ . For a locally finite process we can define the count function  $N(B) = \#(X \cap B)$ , which characterizes the distribution of the process. A Poisson process is a locally finite process for which there exists a locally integrable function  $\lambda : \mathcal{S} \rightarrow [0, \infty)$ , called the intensity function,

such that (i)  $N(B)$  has a Poisson distribution with rate  $\int_B \lambda(t, \mathbf{s}) dt ds$ , and (ii) for disjoint sets  $B_1, \dots, B_k$  the random variables  $N(B_1), \dots, N(B_k)$  are independent. A consequence of (i) and (ii) is that the conditional distribution of the points in  $X \cap B$  given  $N(B) = m$  is the distribution of  $m$  independent and identically distributed observations with density  $\lambda(t, \mathbf{s}) / \int_B \lambda$ .

It follows that for a realization  $x = \{(t_1, \mathbf{s}_1), \dots, (t_m, \mathbf{s}_m)\}$  of a Poisson process  $X$  on a given bounded region  $B = B_t \times B_s$  the density function (in the sense of Proposition 3.1 of Møller and Waagepetersen, 2004) is

$$f(x) = \frac{\exp(-\int_B \lambda)}{m!} \prod_{j=1}^m \lambda(t_j, \mathbf{s}_j). \quad (1)$$

For replicated point processes, a single intensity function  $\lambda$  rarely provides an adequate fit for all replications; it is more reasonable to assume that  $\lambda$  itself is random. Such processes are called doubly stochastic or Cox processes (Møller and Waagepetersen, 2004, ch. 5; Streit, 2010, ch. 8). A doubly stochastic Poisson process is a pair  $(X, \Lambda)$  where  $X | \Lambda = \lambda$  is a Poisson process with intensity function  $\lambda$ , and  $\Lambda$  is a random function that takes values on the space  $\mathcal{F}$  of non-negative locally integrable functions on  $\mathcal{S}$ .

We assume  $\Lambda(t, \mathbf{s})$  factorizes as

$$\Lambda(t, \mathbf{s}) = R \Lambda_t(t) \Lambda_s(\mathbf{s}) \quad (2)$$

for a temporal process  $\Lambda_t$ , a spatial process  $\Lambda_s$  and a random scale factor  $R$ . Identifiability constraints for this factorization are discussed below. Factorization (2) implies that the overall rate, the distribution of the temporal points and the distribution of the spatial points are conditionally independent given  $\Lambda = \lambda$ . Therefore the inter-dependence among these three elements is determined by the dependence structure of  $R$ ,  $\Lambda_t$  and  $\Lambda_s$ .

The scale factor  $R$  and the latent processes  $\Lambda_t$  and  $\Lambda_s$  are non-negative, so for simplicity we will assume they are positive and model their logarithms:

$$\log R = \tau + Z, \quad (3)$$

where  $Z$  is a zero-mean random variable,

$$\log \Lambda_t(t) = \mu(t) + \sum_{k=1}^{p_1} U_k \phi_k(t) \quad (4)$$

and

$$\log \Lambda_s(\mathbf{s}) = \nu(\mathbf{s}) + \sum_{k=1}^{p_2} V_k \psi_k(\mathbf{s}), \quad (5)$$

where the  $\phi_k$ s and  $\psi_k$ s are orthonormal functions in  $L^2(B_t)$  and  $L^2(B_s)$ , respectively,  $E(U_k) = E(V_k) = 0$  for all  $k$ , and  $\text{cov}(U_k, U_{k'}) = \text{cov}(V_k, V_{k'}) = 0$  for all  $k \neq k'$ . The terms in (4) and (5) are arranged in decreasing order of variances,  $\sigma_{u_k}^2 = \text{var}(U_k)$  and  $\sigma_{v_k}^2 = \text{var}(V_k)$ . Note that for any processes  $\log \Lambda_t \in L^2(B_t)$  with  $E(\|\log \Lambda_t\|^2) < \infty$  and  $\log \Lambda_s \in L^2(B_s)$  with  $E(\|\log \Lambda_s\|^2) < \infty$ , expansions (4) and (5) always hold with possibly infinite  $p_1$  and  $p_2$ , and are known as Karhunen–Loève expansions (Ash and Gardner, 1975, ch. 1.4). By taking finite  $p_1$  and  $p_2$  in (4) and (5) we do not lose much in practice, since we are mainly interested in smooth processes where the first few components dominate.

Factorization (2) needs some additional constraints for identifiability. It would seem natural to require that  $\Lambda_t$  and  $\Lambda_s$  integrate to one, so the overall rate of the process would be  $R$ , and  $\Lambda_t$  and  $\Lambda_s$  would be probability density functions. Unfortunately those constraints are not well adapted to the log-linear models (4) and (5). For computational simplicity, we will ask instead that  $\log \Lambda_t$  and  $\log \Lambda_s$  integrate to zero, for which it is sufficient to ask that  $\mu$ , the  $\phi_k$ s,  $\nu$  and the  $\psi_k$ s integrate to zero. These constraints are computationally easy to handle. Under these conditions, we have

$$\log R = \frac{1}{|B|} \iint_B \log \Lambda(t, \mathbf{s}) \, dt \, ds,$$

$$\log \Lambda_t(t) = \frac{1}{|B_s|} \int_{B_s} \log \Lambda(t, \mathbf{s}) \, ds - \frac{1}{|B|} \iint_B \log \Lambda(t, \mathbf{s}) \, dt \, ds$$

and

$$\log \Lambda_s(\mathbf{s}) = \frac{1}{|B_t|} \int_{B_t} \log \Lambda(t, \mathbf{s}) \, dt - \frac{1}{|B|} \iint_B \log \Lambda(t, \mathbf{s}) \, dt \, ds,$$

where  $|\cdot|$  denotes Lebesgue measure of the respective sets.

From (4) and (5) it follows that the dependence between  $R$ ,  $\Lambda_t$  and  $\Lambda_s$  is determined by the dependence between  $Z$ ,  $\mathbf{U} = (U_1, \dots, U_{p_1})^T$  and  $\mathbf{V} = (V_1, \dots, V_{p_2})^T$ .

To model this dependence we collect these random effects into a single vector  $\mathbf{W} = (Z, \mathbf{U}^T, \mathbf{V}^T)^T$ , which we assume to follow a multivariate normal distribution with mean zero and covariance matrix

$$\Sigma = \begin{pmatrix} \sigma_z^2 & \boldsymbol{\sigma}_{zu}^T & \boldsymbol{\sigma}_{zv}^T \\ \boldsymbol{\sigma}_{zu} & \text{diag}(\boldsymbol{\sigma}_u^2) & \boldsymbol{\Sigma}_{uv} \\ \boldsymbol{\sigma}_{zv} & \boldsymbol{\Sigma}_{uv}^T & \text{diag}(\boldsymbol{\sigma}_v^2) \end{pmatrix},$$

where  $\boldsymbol{\sigma}_u^2 = (\sigma_{u1}^2, \dots, \sigma_{up_1}^2)$ ,  $\boldsymbol{\sigma}_v^2 = (\sigma_{v1}^2, \dots, \sigma_{vp_2}^2)$ ,  $\boldsymbol{\sigma}_{zu} = \text{cov}(Z, \mathbf{U})$ ,  $\boldsymbol{\sigma}_{zv} = \text{cov}(Z, \mathbf{V})$  and  $\boldsymbol{\Sigma}_{uv} = \text{cov}(\mathbf{U}, \mathbf{V})$ . The main parameters of interest here are the cross-covariances  $\boldsymbol{\sigma}_{zu}$ ,  $\boldsymbol{\sigma}_{zv}$  and  $\boldsymbol{\Sigma}_{uv}$ , since they determine the dependence or independence of the random effects  $Z$ ,  $U_k$ s and  $V_k$ s. In Section 4 we derive the asymptotic distribution of the estimators of these parameters with the main goal of obtaining tests and confidence intervals for inference. Of secondary importance, but still useful, are confidence intervals for the variances  $\sigma_{uk}^2$ s and  $\sigma_{vk}^2$ s, since variances that are not significantly different from zero would indicate that the respective components superfluous.

To facilitate estimation of the functional parameters  $\mu$ ,  $\nu$ ,  $\phi_k$ s and  $\psi_k$ s, we will use semiparametric basis-function expansions. As basis functions for the temporal elements we will use  $B$ -splines, and for the spatial elements we will use renormalized Gaussian radial kernels. But other families could be used, like simplicial bases for irregular spatial domains; our derivations in this paper are not tied down to any specific bases. We will call these families  $\mathcal{B}_t$  and  $\mathcal{B}_s$ , respectively. Let  $\boldsymbol{\beta}_t(t)$  be the vector of  $q_1$  basis functions of  $\mathcal{B}_t$  and  $\boldsymbol{\beta}_s(\mathbf{s})$  the vector of  $q_2$  basis functions of  $\mathcal{B}_s$ . Then we assume  $\mu(t) = \mathbf{c}_0^T \boldsymbol{\beta}_t(t)$ ,  $\phi_k(t) = \mathbf{c}_k^T \boldsymbol{\beta}_t(t)$ ,  $\nu(\mathbf{s}) = \mathbf{d}_0^T \boldsymbol{\beta}_s(\mathbf{s})$ , and  $\psi_k(\mathbf{s}) = \mathbf{d}_k^T \boldsymbol{\beta}_s(\mathbf{s})$ . The orthonormality constraints on the  $\phi_k$ s can be expressed as  $\mathbf{c}_k^T \mathbf{J}_t \mathbf{c}_{k'} = \delta_{kk'}$ , where  $\delta_{kk'}$  is Kronecker's delta and  $\mathbf{J}_t = \int_{B_t} \boldsymbol{\beta}_t(t) \boldsymbol{\beta}_t(t)^T dt$ , and similarly for the  $\psi_k$ s. The zero-integral constraints for  $\mu$  and the  $\phi_k$ s can be expressed as  $\mathbf{a}_{t0}^T \mathbf{c}_k = 0$  for  $k = 0, \dots, p_1$ , where  $\mathbf{a}_{t0} = \int_{B_t} \boldsymbol{\beta}_t(t) dt$ , and similarly for  $\nu$  and the  $\psi_k$ s. For some applications, such as the bike data mentioned in the Introduction, it is also natural to require that the temporal intensity functions and their derivatives match at the endpoints of  $B_t$ . So, if  $B_t = [t_l, t_u]$ , we also have the constraints  $\mu(t_l) = \mu(t_u)$ ,  $\mu'(t_l) = \mu'(t_u)$ ,  $\phi_k(t_l) = \phi_k(t_u)$  and  $\phi_k'(t_l) = \phi_k'(t_u)$  for all  $k$ , which can be expressed as  $\mathbf{A}_P \mathbf{c}_k = \mathbf{0}$  for  $k = 0, \dots, p_1$ , with  $\mathbf{A}_P = [\boldsymbol{\beta}_t(t_u) - \boldsymbol{\beta}_t(t_l), \boldsymbol{\beta}'_t(t_u) - \boldsymbol{\beta}'_t(t_l)]^T$ .

### 3 Parameter estimation

#### 3.1 Penalized maximum likelihood estimation

For simplicity of notation we collect all model parameters into a single vector

$$\boldsymbol{\theta} = (\boldsymbol{\sigma}_{zu}, \boldsymbol{\sigma}_{zv}, \text{vec } \boldsymbol{\Sigma}_{uv}, \tau, \sigma_z^2, \mathbf{c}_0, \text{vec } \mathbf{C}, \boldsymbol{\sigma}_u^2, \mathbf{d}_0, \text{vec } \mathbf{D}, \boldsymbol{\sigma}_v^2), \quad (6)$$

where  $\mathbf{C} = [\mathbf{c}_1, \dots, \mathbf{c}_{p_1}]$  and  $\mathbf{D} = [\mathbf{d}_1, \dots, \mathbf{d}_{p_2}]$ . From the distributional assumptions in Section 2, the joint density of  $(x, \mathbf{w})$  can be factorized as

$$f_{\boldsymbol{\theta}}(x, \mathbf{w}) = f_{\boldsymbol{\theta}}(x | \mathbf{w})f_{\boldsymbol{\theta}}(\mathbf{w})$$

with  $f_{\boldsymbol{\theta}}(x | \mathbf{w})$  as in (1) and  $f_{\boldsymbol{\theta}}(\mathbf{w})$  the multivariate normal density. Explicitly,

$$f_{\boldsymbol{\theta}}(x | \mathbf{w}) = \frac{\exp\{-rI_t(\mathbf{u})I_s(\mathbf{v})\}}{m!} r^m \prod_{j=1}^m \lambda_t(t_j; \mathbf{u}) \prod_{j=1}^m \lambda_s(\mathbf{s}_j; \mathbf{v}),$$

where  $r = \exp(\tau + z)$ ,  $\lambda_t(t; \mathbf{u}) = \exp\{\mu(t) + \mathbf{u}^T \boldsymbol{\phi}(t)\}$ ,  $\lambda_s(\mathbf{s}; \mathbf{v}) = \exp\{\nu(\mathbf{s}) + \mathbf{v}^T \boldsymbol{\psi}(\mathbf{s})\}$ ,  $I_t(\mathbf{u}) = \int_{B_t} \lambda_t(t; \mathbf{u}) dt$ , and  $I_s(\mathbf{v}) = \int_{B_s} \lambda_s(\mathbf{s}; \mathbf{v}) ds$ . The marginal density for the observable datum  $x$  is

$$f_{\boldsymbol{\theta}}(x) = \int f_{\boldsymbol{\theta}}(x, \mathbf{w}) d\mathbf{w},$$

which has no closed form. We use Laplace's approximation for its evaluation, as explained in the Supplementary Material.

Given  $n$  independent realizations  $x_1, \dots, x_n$  of the process  $X$ , the maximum likelihood estimator of  $\boldsymbol{\theta}$  would be the maximizer of  $\sum_{i=1}^n \log f_{\boldsymbol{\theta}}(x_i)$ . However, when the basis families  $\mathcal{B}_t$  and  $\mathcal{B}_s$  have large dimensions, it is advisable to regularize the estimators by adding roughness penalties to the objective function. We then define the penalized log-likelihood function

$$\ell_n(\boldsymbol{\theta}) = \frac{1}{n} \sum_{i=1}^n \log f_{\boldsymbol{\theta}}(x_i) - \xi_1 P(\mu) - \xi_2 \sum_{k=1}^{p_1} P(\phi_k) - \xi_3 P(\nu) - \xi_4 \sum_{k=1}^{p_2} P(\psi_k), \quad (7)$$

where the  $\xi$ s are nonnegative smoothing parameters and the  $P(f)$ s are roughness penalty functions. For the temporal functions  $\mu$  and  $\phi_k$ s we use  $P(f) = \int (f'')^2$ , and for the spatial functions  $\nu$  and  $\psi_k$ s we use  $P(f) = \iint \left\{ \left( \frac{\partial^2 f}{\partial s_1^2} \right)^2 + 2 \left( \frac{\partial^2 f}{\partial s_1 \partial s_2} \right)^2 + \left( \frac{\partial^2 f}{\partial s_2^2} \right)^2 \right\}$ .

The estimator of  $\boldsymbol{\theta}$  is then defined as

$$\hat{\boldsymbol{\theta}} = \arg \max_{\boldsymbol{\theta} \in \Theta} \ell_n(\boldsymbol{\theta}),$$

where  $\Theta$  is the parameter space that includes all the constraints discussed in Section 2:

$$\begin{aligned} \Theta = \{ & \boldsymbol{\theta} \in \mathbb{R}^r : h_{kl}^C(\boldsymbol{\theta}) = 0, k = 1, \dots, l, l = 1, \dots, p_1; \\ & h_{kl}^D(\boldsymbol{\theta}) = 0, k = 1, \dots, l, l = 1, \dots, p_2; \mathbf{a}_{t0}^T \mathbf{c}_k = 0, k = 0, \dots, p_1; \\ & \mathbf{a}_{s0}^T \mathbf{d}_k = 0, k = 0, \dots, p_2; \mathbf{A}_P \mathbf{c}_k = 0, k = 0, \dots, p_1; \boldsymbol{\Sigma} > 0\}, \end{aligned} \quad (8)$$

with  $r$  the dimension of  $\boldsymbol{\theta}$ ,  $h_{kl}^C(\boldsymbol{\theta}) = \mathbf{c}_k^T \mathbf{J}_t \mathbf{c}_l - \delta_{kl}$ ,  $h_{kl}^D(\boldsymbol{\theta}) = \mathbf{d}_k^T \mathbf{J}_s \mathbf{d}_l - \delta_{kl}$ , and  $\boldsymbol{\Sigma} > 0$  denoting that  $\boldsymbol{\Sigma}$  is symmetric positive definite. The periodicity constraints  $\mathbf{A}_P \mathbf{c}_k = 0$  need not be present in every situation, but for generality we include them in all our derivations; the results below are still valid if these constraints are simply deleted.

Once  $\hat{\boldsymbol{\theta}}$  has been obtained, individual predictors of the latent random effects  $\mathbf{w}$  can be obtained as  $\hat{\mathbf{w}}_i = E_{\hat{\boldsymbol{\theta}}}(\mathbf{w} \mid x_i)$ . The estimating equations for  $\hat{\boldsymbol{\theta}}$  and an EM algorithm (Dempster et al., 1977) for its computation are derived in the Supplementary Material. Programs implementing these algorithms are available on the author's website.

### 3.2 Choice of meta-parameters

The proposed model has a number of tuning parameters that have to be chosen by the user: (i) the number of functional components  $p_1$  and  $p_2$ , (ii) the basis families  $\mathcal{B}_t$  and  $\mathcal{B}_s$  and in particular their dimensions  $q_1$  and  $q_2$ , and (iii) the smoothing parameters  $\xi$ s. Regarding (ii) we can say that the overall dimensions  $q_1$  and  $q_2$  of the basis families are more relevant parameters than the specifics of the basis functions such as e.g. the precise knot placement or the degree of the polynomials used for a spline family. The dimensions of  $\mathcal{B}_t$  and  $\mathcal{B}_s$  should be chosen relatively large in order to avoid bias; the variability of the estimators will be taken care of by the  $\xi$ s. As noted by Ruppert (2002, sec. 3), although optimal  $q_1$  and  $q_2$  could be chosen by cross-validation (Hastie et al., 2009, ch. 7), there is little change in goodness of fit after a minimum dimension has been reached, and the fit is essentially determined by the smoothing parameters thereafter.

The choice of the smoothing parameters  $\xi$ s is then more important. It can be done objectively by cross-validation. Leave-one-out cross-validation finds  $\xi$ s that maximize

$$\text{CV}(\xi_1, \xi_2, \xi_3, \xi_4) = \sum_{i=1}^n \log f_{\hat{\theta}^{[-i]}}(x_i), \quad (9)$$

where  $\hat{\theta}^{[-i]}$  denotes the estimator obtained without observation  $x_i$ . A faster alternative is to use  $k$ -fold cross-validation, where the data is split into  $k$  subsets that are alternatively used as test data;  $k = 5$  is a common choice. Full four-dimensional optimization of (9) is too time consuming even for five-fold cross-validation; a workable alternative is sequential optimization, where each  $\xi_j$  in turn is optimized on a grid while the other  $\xi$ s are kept fixed at an initial value chosen by the user. A faster but subjective alternative is to choose the  $\xi$ s by visual inspection. Plots of the means and the components for different  $\xi$ s can be inspected to see how new features of the curves appear or disappear as  $\xi$  decreases or increases; the  $\xi$ s that produce curves with well-defined but not too irregular features can then be chosen. Curve shapes change smoothly with  $\xi$ , so there is usually a relatively broad range of  $\xi$ s that will produce comparable and reasonable results; there is no need to select the exact optimal  $\xi$ .

The choice of the number of components  $p_1$  and  $p_2$  can also be done either objectively or subjectively, the former by cross-validation or testing, the latter by taking into account the relative contributions of the new components on the total variances,  $\sigma_{up_1}^2 / (\sigma_{u1}^2 + \dots + \sigma_{up_1}^2)$  and  $\sigma_{vp_2}^2 / (\sigma_{v1}^2 + \dots + \sigma_{vp_2}^2)$ .

## 4 Asymptotics

The asymptotic behavior of  $\hat{\theta}$  as  $n \rightarrow \infty$  can be studied via empirical-process techniques (Pollard, 1984; Van der Vaart, 2000), since (7) is the average of independent identically distributed functions plus non-random roughness penalties, as in e.g. Knight and Fu (2000). We will develop here a ‘parametric’ asymptotics where the dimensions  $q_1$  and  $q_2$  of the basis families  $\mathcal{B}_t$  and  $\mathcal{B}_s$  are held fixed and the true functional parameters are assumed to belong to  $\mathcal{B}_t$  and  $\mathcal{B}_s$ . This assumption, in practice, is not very unrealistic as long as  $q_1$  and  $q_2$  are reasonably large. Other authors have followed this ‘parametric’ asymptotic approach in similar semiparametric contexts (e.g. Yu and Ruppert, 2002, and Xun et al., 2013).

The first result of this section, Theorem 1, establishes consistency of the estimator  $\hat{\boldsymbol{\theta}}$ . The proof is given in the Supplementary Material. For uniqueness of the true parameters, the indeterminate signs of the  $\phi_k$ s and  $\psi_k$ s require special handling; we also need to assume that the components have multiplicity one. Our modified parameter space, then, will be

$$\begin{aligned} \Theta = \{ & \boldsymbol{\theta} \in \mathbb{R}^r : h_{kl}^C(\boldsymbol{\theta}) = 0, k = 1, \dots, l, l = 1, \dots, p_1; \\ & h_{kl}^D(\boldsymbol{\theta}) = 0, k = 1, \dots, l, l = 1, \dots, p_2; \mathbf{a}_{t0}^T \mathbf{c}_k = 0, k = 0, \dots, p_1; \\ & \mathbf{a}_{s0}^T \mathbf{d}_k = 0, k = 0, \dots, p_2; \mathbf{A}_P \mathbf{c}_k = 0, k = 0, \dots, p_1; \\ & \boldsymbol{\Sigma} > \mathbf{0}; \sigma_{u1} > \dots > \sigma_{up_1} > 0; \sigma_{v1} > \dots > \sigma_{vp_2} > 0; \\ & c_{k1} \geq 0, k = 1, \dots, p_1; d_{k1} \geq 0, k = 1, \dots, p_2\}. \end{aligned} \quad (10)$$

We make the following assumptions:

- A1** The signs of the  $\hat{\phi}_k$ s and  $\hat{\psi}_k$ s are specified so that the first non-zero basis coefficient of each  $\hat{\phi}_k$  and  $\hat{\psi}_k$  is positive (then  $\hat{\boldsymbol{\theta}} \in \Theta$  for  $\Theta$  defined in (10).)
- A2** The true functional parameters  $\mu_0, \nu_0, \phi_{k0}$ s and  $\psi_{k0}$ s of models (4) and (5) belong to the functional spaces  $\mathcal{B}_t$  and  $\mathcal{B}_s$ , and their basis coefficients  $c_{k1,0}$  and  $d_{k1,0}$  are not zero. The signs of  $\phi_{k0}$  and  $\psi_{k0}$  are then chosen so that  $c_{k1,0} > 0$  and  $d_{k1,0} > 0$ ; therefore there is a unique  $\boldsymbol{\theta}_0$  in  $\Theta$  such that  $f_{\boldsymbol{\theta}_0}(x)$  is the true density of the data.
- A3**  $\boldsymbol{\xi}_n \rightarrow \mathbf{0}$  as  $n \rightarrow \infty$ , where  $\boldsymbol{\xi}_n = (\xi_{1n}, \xi_{2n}, \xi_{3n}, \xi_{4n})^T$  is the vector of smoothing parameters in (7).

The requirement, in assumption A2, that the first basis coefficients  $c_{k1,0}$  and  $d_{k1,0}$  of each  $\phi_{k0}$  and  $\psi_{k0}$  be non-zero is somewhat artificial: although the  $\phi_{k0}$ s and  $\psi_{k0}$ s must have at least one non-zero basis coefficient, it need not be the first one. However, a condition like this is necessary to uniquely identify a ‘true’ parameter  $\boldsymbol{\theta}_0$ , which would otherwise be unidentifiable due to sign ambiguity, and that condition has to be consistent with a sign-specification rule that can be used for the estimators, such as the one in assumption A1.

**Theorem 1** *Under assumptions A1–A3,  $\hat{\boldsymbol{\theta}} \xrightarrow{P} \boldsymbol{\theta}_0$  as  $n \rightarrow \infty$ .*

To establish asymptotic normality of the estimators we will use the results of Geyer (1994), which make use of the tangent cone of the parameter space. The definition and properties of tangent cones can be found in Rockafellar and Wets (1998, ch. 6). From Theorem 6.31 of Rockafellar and Wets (1998), the tangent cone of  $\Theta$  at  $\boldsymbol{\theta}_0$  is

$$\begin{aligned}\mathcal{T}_0 &= \{\boldsymbol{\delta} \in \mathbb{R}^r : \nabla h_{kl}^C(\boldsymbol{\theta}_0)^T \boldsymbol{\delta} = 0, k = 1, \dots, l, l = 1, \dots, p_1; \\ &\quad \nabla h_{kl}^D(\boldsymbol{\theta}_0)^T \boldsymbol{\delta} = 0, k = 1, \dots, l, l = 1, \dots, p_2; \quad \mathbf{a}_{t_0}^T \mathbf{K}_{\mathbf{c}_k} \boldsymbol{\delta} = 0, k = 0, \dots, p_1; \\ &\quad \mathbf{a}_{s_0}^T \mathbf{K}_{\mathbf{d}_k} \boldsymbol{\delta} = 0, k = 0, \dots, p_2; \quad \mathbf{A}_P \mathbf{K}_{\mathbf{c}_k} \boldsymbol{\delta} = 0, k = 0, \dots, p_1\},\end{aligned}$$

where  $\mathbf{K}_{\mathbf{d}_k}$  and  $\mathbf{K}_{\mathbf{c}_k}$  are the ‘extraction’ matrices such that  $\mathbf{d}_k = \mathbf{K}_{\mathbf{d}_k} \boldsymbol{\theta}$  and  $\mathbf{c}_k = \mathbf{K}_{\mathbf{c}_k} \boldsymbol{\theta}$ . The explicit forms of  $\nabla h_{kl}^C(\boldsymbol{\theta})$  and  $\nabla h_{kl}^D(\boldsymbol{\theta})$  are derived in the Supplementary Material. Let  $\mathbf{A}$  be the  $r_1 \times r$  matrix with rows  $\nabla h_{kl}^C(\boldsymbol{\theta}_0)^T$ ,  $\nabla h_{kl}^D(\boldsymbol{\theta}_0)^T$ ,  $\mathbf{a}_{t_0}^T \mathbf{K}_{\mathbf{c}_k}$ ,  $\mathbf{a}_{s_0}^T \mathbf{K}_{\mathbf{d}_k}$  and  $\mathbf{A}_P \mathbf{K}_{\mathbf{c}_k}$ , and let  $\mathbf{B}$  be an orthogonal complement of  $\mathbf{A}$ , that is, an  $(r - r_1) \times r$  matrix such that  $\mathbf{A}\mathbf{B}^T = \mathbf{O}$ .

The next theorem gives the asymptotic distribution of  $\hat{\boldsymbol{\theta}}$ . In addition to  $\mathbf{B}$  above, it uses Fisher’s information matrix,

$$\begin{aligned}\mathbf{F}_0 &= E_{\boldsymbol{\theta}_0} \{\nabla \log f_{\boldsymbol{\theta}_0}(X) \nabla \log f_{\boldsymbol{\theta}_0}(X)^T\} \\ &= -E_{\boldsymbol{\theta}_0} \{\nabla^2 \log f_{\boldsymbol{\theta}_0}(X)\},\end{aligned}$$

where  $\nabla$  and  $\nabla^2$  are taken with respect to the parameter  $\boldsymbol{\theta}$ , and  $\mathbf{D}\mathbf{P}(\boldsymbol{\theta})$ , the Jacobian matrix of the smoothness penalty vector  $\mathbf{P}(\boldsymbol{\theta}) = (P(\mu), \sum_{k=1}^{p_1} P(\phi_k), P(\nu), \sum_{k=1}^{p_2} P(\psi_k))^T$ . Explicit expressions for these derivatives are given in the Supplementary Material. We also need an additional assumption:

**A4**  $\sqrt{n}\boldsymbol{\xi}_n \rightarrow \boldsymbol{\kappa}$  as  $n \rightarrow \infty$ , for a finite  $\boldsymbol{\kappa}$ .

**Theorem 2** *Under assumptions A1–A4,  $\sqrt{n}(\hat{\boldsymbol{\theta}} - \boldsymbol{\theta}_0) \xrightarrow{D} \mathbf{N}(-\mathbf{V}\mathbf{D}\mathbf{P}(\boldsymbol{\theta}_0)^T \boldsymbol{\kappa}, \mathbf{V})$  as  $n \rightarrow \infty$ , with  $\mathbf{V} = \mathbf{B}^T(\mathbf{B}\mathbf{F}_0\mathbf{B}^T)^{-1}\mathbf{B}$ .*

Fisher’s information matrix  $\mathbf{F}_0$  can be estimated by

$$\hat{\mathbf{F}}_0 = \frac{1}{n} \sum_{i=1}^n \nabla \log f_{\hat{\boldsymbol{\theta}}}(x_i) \nabla \log f_{\hat{\boldsymbol{\theta}}}(x_i)^T \quad (11)$$

and  $\mathbf{V}$  in Theorem 2 by  $\hat{\mathbf{V}} = \mathbf{B}^T(\mathbf{B}\hat{\mathbf{F}}_0\mathbf{B}^T)^{-1}\mathbf{B}$ . Due to the high dimensionality of  $\boldsymbol{\theta}$ ,  $\hat{\mathbf{F}}_0$  is often singular or nearly singular for small sample sizes, leading to unstable values of  $\hat{\mathbf{V}}$ . In such cases, a practical alternative is to treat the functional parameters  $\mu$ ,  $\nu$ ,  $\phi_k$ s and  $\psi_k$ s as if they were fixed and known, reducing  $\boldsymbol{\theta}$  to a more manageable  $\tilde{\boldsymbol{\theta}} = (\sigma_{zu}, \sigma_{zv}, \text{vec } \boldsymbol{\Sigma}_{uv}, \tau, \sigma_z^2, \sigma_u^2, \sigma_v^2)$ . Fisher's information matrix for  $\tilde{\boldsymbol{\theta}}$ ,  $\tilde{\mathbf{F}}_0$ , is usually low-dimensional enough that it can be accurately estimated by the corresponding version of (11),  $\hat{\tilde{\mathbf{F}}}_0$ , even for relatively small sample sizes. Note that since  $\tilde{\boldsymbol{\theta}}$  is not subject to equality constraints or smoothness penalties, the asymptotic distribution of  $\sqrt{n}(\hat{\tilde{\boldsymbol{\theta}}} - \tilde{\boldsymbol{\theta}}_0)$  is simply  $N(\mathbf{0}, \hat{\tilde{\mathbf{F}}}_0^{-1})$ , the standard maximum likelihood asymptotics. The functional parameters  $\mu$ ,  $\nu$ ,  $\phi_k$ s and  $\psi_k$ s still need to be estimated, of course, since they must be plugged into  $\hat{\tilde{\mathbf{F}}}_0$ . This 'reduced' or 'marginal' asymptotics produces accurate variance estimators even for small sample sizes, as shown by simulation in Section 5.

## 5 Simulations

To assess the finite-sample behavior of the estimators, we generated data from model (3)-(4)-(5) with  $p_1 = p_2 = 2$ . We took the interval  $B_t = [0, 1]$  as temporal domain, and functional parameters  $\mu(t) = \sin \pi t - c_1$ ,  $\phi_1(t) = (\sin \pi t - c_1)/c_2$  and  $\phi_2(t) = \sqrt{2} \sin 2\pi t$ , where  $c_1$  and  $c_2$  are standardizing constants. As spatial domain we took the rectangle  $B_s = [0, 1] \times [0, 1]$ , and functional parameters  $\nu(s_1, s_2) = -(s_1 - .5)^2 - (s_2 - .5)^2 - c_3$ ,  $\psi_1(s_1, s_2) = \{\sin(\pi s_1) \sin(\pi s_2) - c_4\}/c_5$  and  $\psi_2(s_1, s_2) = 2 \sin(2\pi s_1) \sin(2\pi s_2)$ , where  $c_3$ ,  $c_4$  and  $c_5$  are standardizing constants. For  $\tau$  we used two different values,  $\tau = \log 10$  and  $\tau = \log 30$ ; the lower  $\tau$  generates sparse data where the individual intensity functions cannot be estimated by individual smoothing.

The variances were taken as  $\sigma_{u1}^2 = .3^2 \times .7$ ,  $\sigma_{u2}^2 = .3^2 \times .3$ ,  $\sigma_{v1}^2 = .7^2 \times .7$  and  $\sigma_{v2}^2 = .7^2 \times .3$ . The cross-covariance parameters were set as  $\boldsymbol{\sigma}_{zu} = \mathbf{0}$ ,  $\boldsymbol{\sigma}_{zv} = \mathbf{0}$  and  $\boldsymbol{\Sigma}_{uv}$  a diagonal matrix with elements  $\boldsymbol{\Sigma}_{uv,11} = .7\sigma_{u1}\sigma_{v1}$  and  $\boldsymbol{\Sigma}_{uv,22} = .7\sigma_{u2}\sigma_{v2}$ , so  $U_1$  and  $U_2$  were correlated with  $V_1$  and  $V_2$ , respectively. We considered four sample sizes  $n$ : 50, 100, 200 and 400. Each scenario was replicated 500 times.

For estimation we used cubic  $B$ -splines with ten equally spaced knots for the temporal functions, and normalized Gaussian kernels with 25 uniformly spaced knots for the spatial functions. This gives dimensions  $q_1 = 14$  and  $q_2 = 25$ , respectively.

Parameter	$\tau$							
	log 10				log 30			
	$n$				$n$			
	50	100	200	400	50	100	200	400
$\sigma_{zu,1}$	.024	.019	.016	.013	.015	.013	.012	.011
$\sigma_{zu,2}$	.016	.011	.009	.007	.012	.008	.006	.004
$\sigma_{zv,1}$	.044	.043	.037	.035	.039	.034	.031	.030
$\sigma_{zv,2}$	.030	.019	.013	.008	.022	.014	.009	.007
$\Sigma_{uv,11}$	.043	.031	.017	.014	.032	.021	.015	.010
$\Sigma_{uv,21}$	.040	.031	.018	.015	.024	.017	.011	.008
$\Sigma_{uv,12}$	.031	.019	.012	.008	.014	.013	.008	.006
$\Sigma_{uv,22}$	.026	.015	.011	.007	.013	.008	.007	.004
$\tau$	.089	.092	.101	.103	.073	.066	.065	.065
$\mu$	.145	.107	.074	.062	.117	.084	.072	.058
$\phi_1$	.551	.425	.243	.180	.365	.249	.157	.116
$\phi_2$	.724	.541	.395	.349	.451	.296	.199	.156
$\nu$	.291	.244	.203	.188	.256	.215	.202	.178
$\psi_1$	.397	.295	.217	.165	.274	.213	.173	.150
$\psi_2$	.582	.424	.315	.249	.372	.267	.204	.171
$\sigma_z$	.068	.049	.037	.027	.051	.030	.022	.018
$\sigma_{u1}$	.045	.034	.021	.018	.036	.024	.017	.012
$\sigma_{u2}$	.040	.032	.026	.022	.030	.021	.016	.011
$\sigma_{v1}$	.060	.057	.050	.040	.062	.047	.034	.031
$\sigma_{v2}$	.047	.028	.021	.016	.037	.027	.022	.017

Table 1: Simulation Results. Root mean squared errors of parameter estimators.

As smoothing parameters we took all  $\xi$ s equal to  $10^{-5}$ .

As measure of estimation error we use the root mean squared error. For scalar parameters, e.g.  $\tau$ , we employ the usual definition,  $\{E(\hat{\tau} - \tau)^2\}^{1/2}$ . For functional parameters, e.g.  $\mu(t)$ , the root mean squared error is defined in terms of the  $L^2$ -norm as  $\{E(\|\hat{\mu} - \mu\|^2)\}^{1/2}$ . For random-effect estimators, e.g. the  $\hat{u}_{i1}$ s, we define it as  $\{E \sum_{i=1}^n (\hat{u}_{i1} - u_{i1})^2/n\}^{1/2}$ . The signs of the  $\hat{\phi}_k$ s and the  $\hat{\psi}_k$ s, which in principle are indeterminate, are chosen as the signs of the inner products  $\langle \hat{\phi}_k, \phi_k \rangle$  and  $\langle \hat{\psi}_k, \psi_k \rangle$ , respectively; the signs of the  $\hat{u}_{iks}$  and  $\hat{v}_{iks}$ , and of the elements of  $\hat{\sigma}_{zu}$ ,  $\hat{\sigma}_{zv}$  and  $\hat{\Sigma}_{uv}$ , are changed accordingly.

Table 1 shows that, as expected, the estimation errors decrease as  $n$  increases, and

Variable	$\tau$							
	log 10				log 30			
	$n$				$n$			
	50	100	200	400	50	100	200	400
$Z$	.244	.242	.232	.230	.179	.174	.174	.170
$U_1$	.200	.180	.171	.167	.158	.144	.138	.135
$U_2$	.169	.157	.148	.144	.132	.121	.116	.114
$V_1$	.298	.282	.271	.265	.239	.215	.211	.196
$V_2$	.274	.247	.237	.230	.189	.173	.162	.157

Table 2: Simulation Results. Root mean squared errors of random-effect estimators.

also decrease as the baseline rate, determined by  $\tau$ , increases. But even in the sparse situation  $\tau = \log 10$  we see that the functional parameters are accurately estimated, which shows the advantages of ‘borrowing strength’ across replications. Somewhat unusual is the case of  $\hat{\tau}$ , whose estimation errors do not decrease as functions of  $n$  as fast as they do for the other parameters. A more in-depth analysis reveals that this is due to bias. Nevertheless,  $\tau$  is not a very important parameter for inferential purposes; more important are the cross-covariance parameters and the functional components, and they are accurately estimated.

Table 2 shows that the estimation errors of the random-effect estimators also decrease as  $n$  increases, but  $\tau$ , which determines the number of observations per individual, has a larger impact here than  $n$  does. The reason is that each random-effect estimator can only be computed from the observations available for each individual; ‘borrowing strength’ across replications is not possible for the random effects.

Tables 3 and 4 compare the true finite-sample standard deviations of the estimators with their mean asymptotic approximations. We use the ‘reduced’ asymptotics mentioned at the end of Section 4, treating the functional parameters as if they were fixed and known. The dimension of the full  $\boldsymbol{\theta}$  is 131, whereas the dimension of the reduced  $\tilde{\boldsymbol{\theta}}$  is 14, so it is clear that only the ‘reduced’ asymptotics is practical for our sample sizes. Tables 3 and 4 show that the true standard deviations of the estimators are accurately estimated, especially for  $n \geq 100$ . Even for  $n = 50$ , where the approximation is not as good for some parameters, the asymptotic standard deviations tend to overestimate the true standard deviations, which, for inferential purposes, is better than underestimating them. For  $n \geq 200$  the approximation is extremely accurate for most parameters, even under the sparse scenario  $\tau = \log 10$ . The accuracy

Parameter	<i>n</i>											
	50			100			200			400		
	True	Mean	Sd	True	Mean	Sd	True	Mean	Sd	True	Mean	Sd
$\text{sd}(\hat{\sigma}_{zu,1})$	.211	.355	.082	.141	.206	.038	.104	.128	.015	.072	.084	.007
$\text{sd}(\hat{\sigma}_{zu,2})$	.160	.291	.061	.115	.163	.023	.088	.100	.011	.066	.065	.006
$\text{sd}(\hat{\sigma}_{zv,1})$	.327	.558	.125	.259	.329	.053	.184	.209	.024	.120	.142	.011
$\text{sd}(\hat{\sigma}_{zv,2})$	.295	.420	.084	.191	.245	.033	.126	.153	.020	.081	.102	.007
$\text{sd}(\hat{\Sigma}_{uw,11})$	.411	.490	.125	.310	.289	.051	.161	.177	.020	.124	.121	.012
$\text{sd}(\hat{\Sigma}_{uw,21})$	.398	.377	.083	.311	.202	.035	.181	.124	.011	.151	.081	.007
$\text{sd}(\hat{\Sigma}_{uw,12})$	.305	.333	.061	.192	.189	.024	.117	.119	.012	.084	.079	.006
$\text{sd}(\hat{\Sigma}_{uw,22})$	.254	.299	.057	.153	.166	.022	.109	.104	.011	.070	.069	.005

Table 3: Simulation Results. Comparison of true and asymptotic standard deviations of the parameter estimators ( $\times 10$ ). For the asymptotic standard deviations, mean and standard deviations are reported. Results for simulations with  $\tau = \log 10$ .

Parameter	$n$											
	50			100			200			400		
	True	Mean	Sd									
$\text{sd}(\hat{\sigma}_{zu,1})$	.144	.207	.045	.095	.127	.018	.077	.086	.009	.056	.058	.005
$\text{sd}(\hat{\sigma}_{zu,2})$	.118	.151	.034	.081	.092	.014	.058	.061	.006	.040	.041	.003
$\text{sd}(\hat{\sigma}_{zv,1})$	.332	.401	.091	.200	.252	.037	.156	.169	.019	.110	.113	.008
$\text{sd}(\hat{\sigma}_{zv,2})$	.217	.269	.056	.141	.169	.022	.092	.111	.012	.071	.076	.006
$\text{sd}(\hat{\Sigma}_{uv,11})$	.322	.373	.099	.209	.223	.041	.147	.151	.020	.096	.101	.010
$\text{sd}(\hat{\Sigma}_{uv,21})$	.240	.200	.037	.169	.121	.018	.108	.079	.009	.078	.054	.004
$\text{sd}(\hat{\Sigma}_{uv,12})$	.139	.185	.041	.125	.110	.013	.082	.073	.006	.057	.050	.004
$\text{sd}(\hat{\Sigma}_{uv,22})$	.130	.162	.033	.081	.100	.015	.066	.067	.007	.041	.045	.003

Table 4: Simulation Results. Comparison of true and asymptotic standard deviations of the parameter estimators ( $\times 10$ ). For the asymptotic standard deviations, mean and standard deviations are reported. Results for simulations with  $\tau = \log 30$ .

of the approximation does not change much with  $\tau$ .

## 6 Application: Chicago’s Divvy bike sharing system

As mentioned in the Introduction, in this section we analyze bike trips that took place between April 1 and November 31 of 2016 in Chicago’s Divvy system. Specifically, we analyze trips originating at station 166, located at the intersection of Wrightwood and Ashland avenues. For each bike trip we observe the time  $t$  when the bike was checked out and its spatial destination  $\mathbf{s}$ , so we can see  $(t, \mathbf{s})$  as an observation from a spatio-temporal process. Strictly speaking,  $\mathbf{s}$  is a discrete variable that can only take values on the lattice of 458 stations, but this grid is dense enough that for practical purposes we can consider  $\mathbf{s}$  as continuous.

For estimation of the temporal functional parameters we used cubic B-splines with ten equally spaced knots in  $B_t = [0, 24]$ , so the family  $\mathcal{B}_t$  had dimension  $q_1 = 14$ . The spatial domain  $B_s$  is more irregular. Since all trips from this station have destinations within the rectangle  $[-87.840, -87.530] \times [41.800, 42.030]$ , we took as  $B_s$  the sector of the city included in this rectangle, which is basically the northern half of the city. As basis family for the spatial functional parameters we used renormalized Gaussian kernels with 43 equally spaced centroids (we created a grid of 100 equally spaced points in the rectangle  $[-87.840, -87.530] \times [41.800, 42.030]$ , and 43 of those ended up within the city boundaries). Then the family  $\mathcal{B}_s$  has dimension  $q_2 = 43$ . As smoothing parameters we took all  $\xi$ s equal to  $10^{-5}$ , which provide smooth estimators while retaining a reasonable level of local detail.

We tried different combinations of numbers of components  $(p_1, p_2)$ :  $(1, 1)$ ,  $(2, 2)$ ,  $(3, 2)$ ,  $(3, 3)$  and  $(4, 4)$ . For each model we computed five-fold cross-validated mean log-likelihoods, obtaining 40.61, 41.23, 41.34, 41.46 and 41.50, respectively. A scree-plot shows that there is a big improvement from the  $(1, 1)$ -model to the  $(2, 2)$ -model, but practically no improvement from the  $(3, 3)$ -model to the  $(4, 4)$ -model. For the  $(3, 3)$ -model the relative contribution of the variances of the spatial components are 82%, 16% and 2%, respectively, so the last component is rather superfluous. For this reason we opted for the  $(2, 2)$ -model, where the relative variance proportions for the temporal components are 67% and 33%, and for the spatial components 75% and

Figure 1: Divvy Data Analysis. Effect of the temporal components on the baseline intensity. (a) First components, (b) second component. Plot shows baseline intensities (solid line), plus (dashed line) and minus (dotted line) a multiple of the component.

25%, respectively.

To interpret the temporal components we plotted  $\exp\{\hat{\mu}(t)\}$  versus  $\exp\{\hat{\mu}(t) \pm c\hat{\phi}_k(t)\}$  for each  $\hat{\phi}_k$ , where  $c$  is a constant chosen for convenient visualization. Figure 1(a) shows that a negative score on the first component corresponds to a sharp morning peak around 7 am, while a positive score is associated with the absence of a morning spike and a higher bike demand in the early afternoon. This component accounts for the difference between weekday and weekend patterns of demand. This is corroborated by a time series plot of the scores  $\hat{u}_{i1}$ , shown in the Supplementary Material, which is strongly weekly periodic with peaks occurring on Sundays and troughs on Thursdays or Wednesdays. Figure 1(b) shows that a negative score on the second component is associated with higher bike demand in the evening, around 6 pm, while a positive score is associated with lower demand at this time. The time series plot of the scores  $\hat{u}_{i2}$  in the Supplementary Material shows a clear seasonal trend, with a minimum at the summer months. So this component is associated with a seasonal pattern of demand.

Spatial components are harder to interpret from static plots, so we provide three-dimensional surface plots here and color contour plots in the Supplementary Material. Figure 2 corresponds to the first component. We see that a positive score corresponds

Figure 2: Divvy Data Analysis. Effect of the first spatial component on the baseline intensity. Plots show baseline intensity minus [(a)] and plus [(b)] a multiple of the component.

to a sharp peak at the bike station itself, meaning that most trips are short and local those days. A negative score is associated with a higher proportion of trips downtown. A time series plot of the  $\hat{v}_{i1}$ s, shown in the Supplementary Material, is strongly weekly periodical, indicating that this component is strongly associated with weekday versus weekend patterns of usage. For the second spatial component, Figure 3 shows that positive scores are associated with days when most trips stay within the neighborhood or downtown, whereas negative scores correspond to days with a higher proportion of faraway trips.

The estimated cross-correlations between temporal and spatial component scores are:  $\text{corr}(U_1, V_1) = .90$ ,  $\text{corr}(U_1, V_2) = .32$ ,  $\text{corr}(U_2, V_1) = -.12$  and  $\text{corr}(U_2, V_2) = .10$ . The asymptotic standard deviations of these estimators, derived from the results in Section 4 using the Delta Method, are .10, .12, .19 and .19, respectively. Therefore only  $\text{corr}(U_1, V_1)$  and  $\text{corr}(U_1, V_2)$  are statistically significant. The high correlation between  $U_1$  and  $V_1$  is not surprising and easy to interpret: on weekdays, there is a higher proportion of bike trips early in the morning with a downtown destination, suggesting that people use bikes for work commute; whereas on weekends, most bike trips take place in the afternoon and tend to stay in the neighborhood.

Figure 3: Divvy Data Analysis. Effect of the second spatial component on the baseline intensity. Plots show baseline intensity minus [(a)] and plus [(b)] a multiple of the component.

## Acknowledgement

This research was partly supported by US National Science Foundation grant DMS 1505780.

## References

- Ash, R.B. and Gardner, M.F. (1975). *Topics in stochastic processes*. Academic Press, New York.
- Baddeley, A. (2007). Spatial point processes and their applications. In *Stochastic Geometry*, Lecture Notes in Mathematics 1892, pp. 1–75. Springer, New York.
- Baddeley, A.J., Møller, R.A., Howard, C.V., and Boyde, A. (1993). Analysis of a three-dimensional point pattern with replication. *Applied Statistics* **42** 641–668.
- Bell, M.L., and Grunwald, G.K. (2004). Mixed models for the analysis of replicated spatial point patterns. *Biostatistics* **5** 633–648.

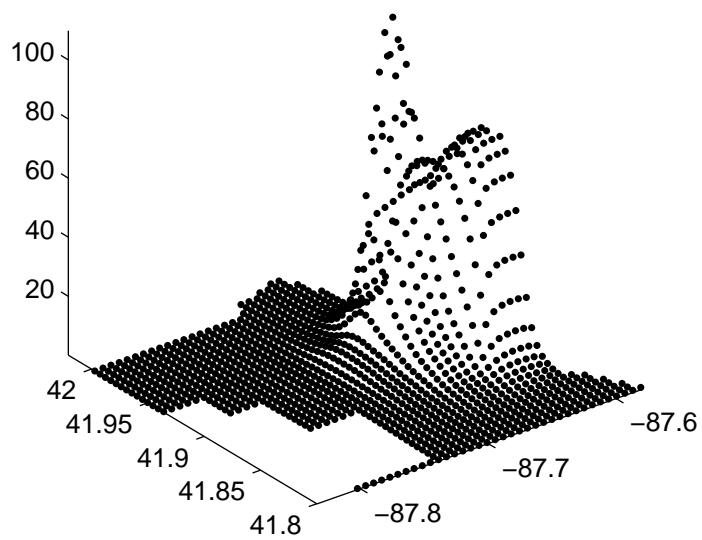
- Bouzas, P.R., Valderrama, M., Aguilera, A.M., and Ruiz-Fuentes, N. (2006). Modelling the mean of a doubly stochastic Poisson process by functional data analysis. *Computational Statistics and Data Analysis* **50** 2655–2667.
- Bouzas, P.R., Ruiz-Fuentes, N., and Ocaña, F.M. (2007). Functional approach to the random mean of a compound Cox process. *Computational Statistics* **22** 467–479.
- Brown, E.N., Kass, R.E. and Mitra, P.P. (2004). Multiple neural spike train data analysis: state-of-the-art and future challenges. *Nature Neuroscience* **7** 456–461.
- Cox, D.R., and Isham, V. (1980). *Point Processes*. Chapman and Hall/CRC, Boca Raton.
- Dempster, A.P., Laird, N.M., and Rubin, D.B. (1977). Maximum likelihood from incomplete data via the EM algorithm. *Journal of the Royal Statistical Society Series B* **39** 1–38.
- Diggle, P.J. (2013). *Statistical Analysis of Spatial and Spatio-Temporal Point Patterns, Third Edition*. Chapman and Hall/CRC, Boca Raton.
- Diggle, P.J., Lange, N., and Beneš, F.M. (1991). Analysis of variance for replicated spatial point patterns in clinical neuroanatomy. *Journal of the American Statistical Association* **86** 618–625.
- Diggle, P.J., Mateau, J., and Clough, H.E. (2000). A comparison between parametric and nonparametric approaches to the analysis of replicated spatial point patterns. *Advances in Applied Probability* **32** 331–343.
- Diggle, P.J., Eglen, S.J., and Troy, J.B. (2006). Modeling the bivariate spatial distribution of amacrine cells. In *Case Studies in Spatial Point Process Modeling*, eds. A. Baddeley et al., New York: Springer, pp. 215–233.
- Fernández-Alcalá, R.M., Navarro-Moreno, J., and Ruiz-Molina, J.C. (2012). On the estimation problem for the intensity of a DSMPP. *Methodology and Computing in Applied Probability* **14** 5–16.

- Gervini, D. (2016). Independent component models for replicated point processes. *Spatial Statistics* **18** 474–488.
- Gervini, D. and Baur, T.J. (2017). Joint models for grid point and response processes in longitudinal and functional data. To appear in *Statistica Sinica* (currently *ArXiv* **1705.06259**).
- Gervini, D. and Khanal, M. (2019). Exploring patterns of demand in bike sharing systems via replicated point process models. *Journal of the Royal Statistical Society Series C: Applied Statistics* **68** 585–602.
- Geyer, C.J. (1994). On the asymptotics of constrained M-estimation. *The Annals of Statistics* **22** 1993–2010.
- Hastie, T., Tibshirani, R., and Friedman, J. (2009). *The Elements of Statistical Learning. Data Mining, Inference, and Prediction. Second Edition*. Springer, New York.
- Knight, K., and Fu, W. (2000). Asymptotics for lasso-type estimators. *The Annals of Statistics* **28** 1356–1378.
- Landau, S., Rabe-Hesketh, S., and Everall, I.P. (2004). Nonparametric one-way analysis of variance of replicated bivariate spatial point patterns. *Biometrical Journal* **46** 19–34.
- Li, Y., and Guan, Y. (2014). Functional principal component analysis of spatiotemporal point processes with applications in disease surveillance. *Journal of the American Statistical Association* **109** 1205–1215.
- Møller, J., and Waagepetersen, R.P. (2004). *Statistical Inference and Simulation for Spatial Point Processes*. Chapman and Hall/CRC, Boca Raton.
- Nair, R., and Miller-Hooks, E. (2011). Fleet management for vehicle sharing operations. *Transportation Science* **45** 524–540.
- Pawlas, Z. (2011). Estimation of summary characteristics from replicated spatial point processes. *Kybernetika* **47** 880–892.
- Pollard, D. (1984). *Convergence of Stochastic Processes*. Springer, New York.

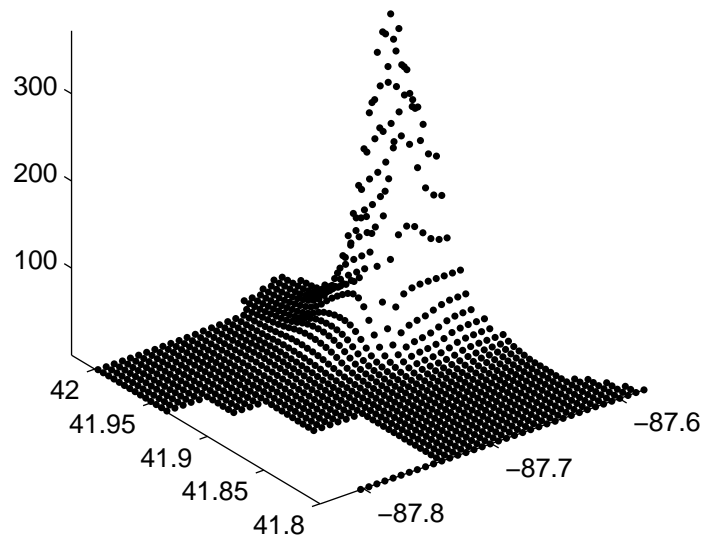
- Ramsay, J.O., and Silverman, B.W. (2005). *Functional Data Analysis (second edition)*. Springer, New York.
- Rockafellar, R.T., and Wets, R.J. (1998). *Variational Analysis*. Springer, New York.
- Ruppert, D. (2002). Selecting the number of knots for penalized splines. *Journal of Computational and Graphical Statistics* **11** 735–757.
- Seber, G.A.F. (2004). *Multivariate Observations*. Wiley, New York.
- Shaheen, S., Guzman, S., and Zhang, H. (2010). Bike sharing in Europe, the Americas and Asia: Past, present and future. *Transportation Research Record: Journal of the Transportation Research Board* **2143** 159–167.
- Shirota, S., and Gelfand, A.E. (2017). Space and circular time log Gaussian Cox processes with application to crime event data. *The Annals of Applied Statistics* **11** 481–503.
- Streit, R.L. (2010). *Poisson Point Processes: Imaging, Tracking, and Sensing*. Springer, New York.
- Van der Vaart, A. (2000). *Asymptotic Statistics*. Cambridge University Press, Cambridge, UK.
- Waagepetersen, R., Guan, Y., Jalilian, A., and Mateu, J. (2016). Analysis of multispecies point patterns by using multivariate log-Gaussian Cox processes. *Journal of the Royal Statistical Society Series C: Applied Statistics* **65** 77–96.
- Wager, C.G., Coull, B.A., and Lange, N. (2004). Modelling spatial intensity for replicated inhomogeneous point patterns in brain imaging. *Journal of the Royal Statistical Society Series B* **66** 429–446.
- Wu, S., Müller, H.-G., and Zhang, Z. (2013). Functional data analysis for point processes with rare events. *Statistica Sinica* **23** 1–23.
- Xun, X., Cao, J., Mallick, B., Maity, A., and Carroll, R.J. (2013). Parameter estimation of partial differential equations. *Journal of the American Statistical Association* **108** 1009–1020.

Yu, Y., and Ruppert, D. (2002). Penalized spline estimation for partially linear single-index models. *Journal of the American Statistical Association* **97** 1042–1054.

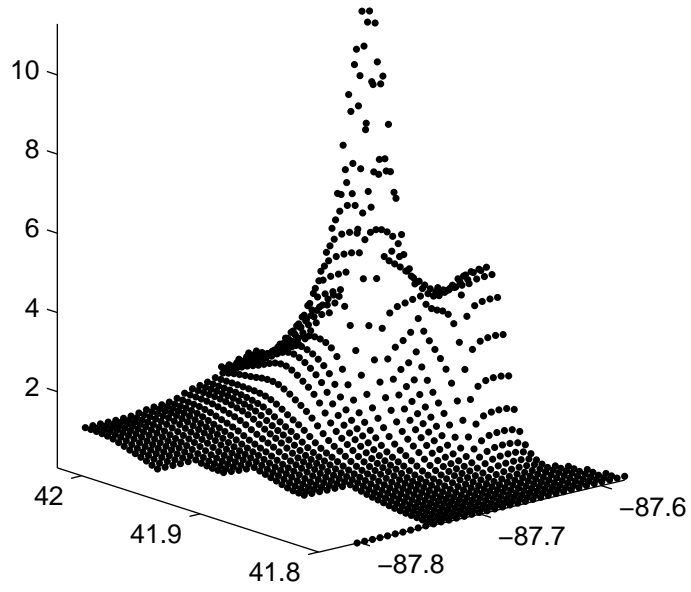
(a)



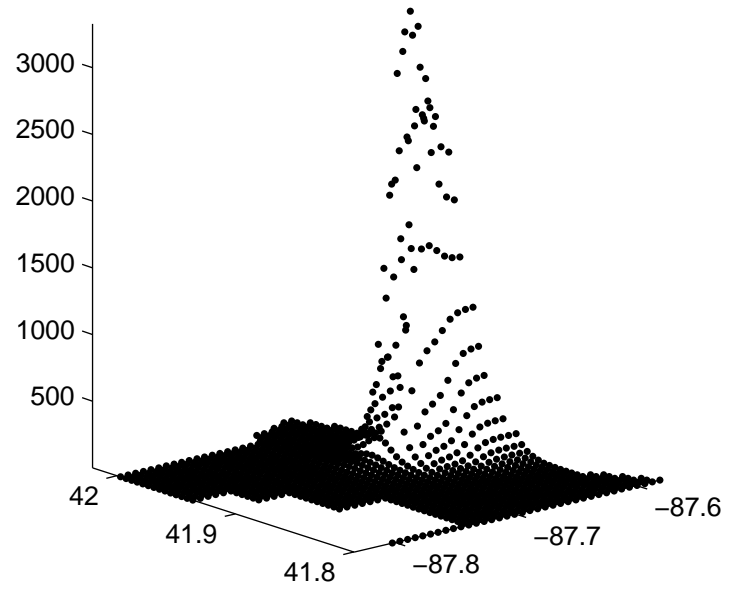
(b)



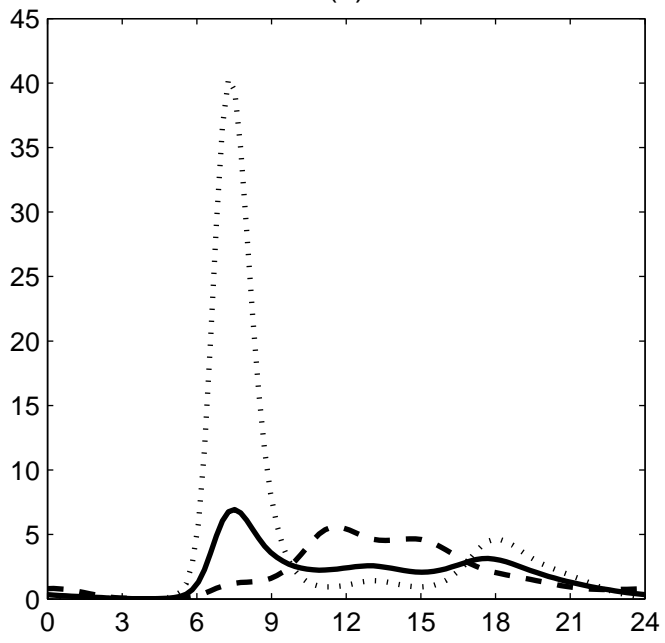
(a)



(b)



(a)



(b)

